

Understanding the effects of root structure on the mechanical behaviour of engineered plant root materials

Carrete, Israel A.; Ghodrat, Sepideh; Scherer, Diana; Karana, Elvin

DOI

[10.1016/j.matdes.2022.111521](https://doi.org/10.1016/j.matdes.2022.111521)

Publication date

2023

Document Version

Final published version

Published in

Materials and Design

Citation (APA)

Carrete, I. A., Ghodrat, S., Scherer, D., & Karana, E. (2023). Understanding the effects of root structure on the mechanical behaviour of engineered plant root materials. *Materials and Design*, 225, Article 111521. <https://doi.org/10.1016/j.matdes.2022.111521>

Important note

To cite this publication, please use the final published version (if applicable). Please check the document version above.

Copyright

Other than for strictly personal use, it is not permitted to download, forward or distribute the text or part of it, without the consent of the author(s) and/or copyright holder(s), unless the work is under an open content license such as Creative Commons.

Takedown policy

Please contact us and provide details if you believe this document breaches copyrights. We will remove access to the work immediately and investigate your claim.



Understanding the effects of root structure on the mechanical behaviour of engineered plant root materials



Israel A. Carrete^a, Sepideh Ghodrat^{a,*}, Diana Scherer^b, Elvin Karana^a

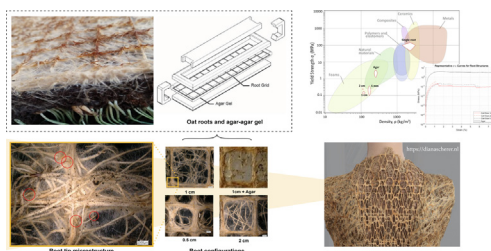
^aMaterializing Futures, Department of Sustainable Design Engineering, Delft University of Technology, Landbergstraat 15, 2628CE Delft, The Netherlands

^bInterwoven, Amsterdam, The Netherlands

HIGHLIGHTS

- A systematic characterization of engineered plant root materials is performed on various configurations.
- Differences in tensile properties between each root configuration suggest there is poor load distribution on root structures.
- Introducing agar-agar as a biopolymer matrix improves tensile properties by homogenizing the load distribution.
- The relationship between structure, root tip density, and material strength implies that properties can be tuned by design.

GRAPHICAL ABSTRACT



ARTICLE INFO

Article history:

Received 19 July 2022

Revised 4 November 2022

Accepted 18 December 2022

Available online 19 December 2022

Keywords:

Engineered Living Materials (ELMs)

Biodesign

Plant Roots

Characterization

Biofabrication

Natural Fiber Composites

Growing Design

Engineered Plant Root Materials (EPRMs)

ABSTRACT

Plant root growth can be altered by introducing obstacles in the path of growth. This principle is used in design to produce planar grid structures composed of interweaving roots. The Engineered Plant Root Materials (EPRMs) grown with this method have the potential to serve as environmentally sensitive alternatives for conventional materials, but their applications are delimited by their material properties. To bridge the gap in the wider application of these materials, the role of plant root structure and an agar-agar matrix are explored in relation to the mechanical properties of the EPRMs. Tensile tests were performed on five root configurations, ranging from single roots to grids of varying sizes. Heterogeneities in each configuration suggest poor load distribution throughout the structure. Agar-agar was introduced as a biopolymer matrix to improve load distribution and tensile properties. Digital microscopy at the intersection of grid cells suggests a correlation between cell size, root tip density, and material strength. The largest cell size (2 cm) had the highest root tip density and yield strength (0.568 ± 0.181 roots/mm² and 0.234 ± 0.018 MPa, respectively), whereas the structure with the least root tips (1 cm) was 31 % weaker.

© 2022 The Authors. Published by Elsevier Ltd. This is an open access article under the CC BY license (<http://creativecommons.org/licenses/by/4.0/>).

1. Introduction

Manufactured materials and natural materials greatly vary in the way they are produced. Natural materials are assembled from

the “bottom up” by singular cells genetically programmed to produce complex structures [1], as opposed to the man-made “top-down” approach. Scientists are now implementing this bottom-up approach to create Engineered Living Materials (ELMs) - materials composed of (or assembled by) living cells through either genetic reprogramming or physical manipulation [2]. ELMs have great potentials for sustainability compared to conventionally

* Corresponding author.

E-mail address: S.Ghodrat@tudelft.nl (S. Ghodrat).

manufactured materials and can be designed through physical or genetic manipulation [3], but scaling up beyond a lab setting poses a challenge to commercialization [2]. The most successfully scaled-up ELMs include physical ELMs that manipulate a system to grow into a design, such as mycelium-based materials [4], and tree shaping [5].

The implementation of physical ELMs has become increasingly common in biodesign, where a combination of biology, design, and engineering are used to produce physical artefacts [6]. Physical ELMs fall into a category known as growing design [7]. This subsection of biodesign provides a sustainable alternative for fabrication methods in design practice [8]. Examples of the organisms used in growing design include bacteria [9], mycelium [10], algae [11], and plants [12,13]. This paper focuses on plant as ELMs. Applications of plant-based materials include the Living Root Bridges, Baubotanik buildings, and Fullgrown furniture (Table 1). Living Root Bridges are structures grown from the roots of *Ficus elastica* trees by the Khasi and Jaintia tribes of Meghalaya, India. The living structures strengthen over time for centuries despite harsh climate conditions. Baubotanik buildings fuse man-made scaffolds with living trees. This results in a “living building” whose organic components continue to grow and strengthen with time [5]. These examples both integrate the growth of the plant into the final structure. Fullgrown, a UK-based company, instead separates the final product from the living organism when growth reaches a certain point. The company shapes trees into wooden furniture, allowing the plant growth to manufacture the product over a period of 6–10 years (<https://fullgrown.co.uk>). The use of plants in biodesign has even brought about alternative textile-like materials, namely Interwoven by Diana Scherer (the 3rd author), grown from plant roots [14].





This paper focuses on plant roots as ELMs by using Interwoven, an Engineered Plant Root Material (EPRM). Scherer mobilizes the growth of plant roots into predefined patterns by introducing obstacles in their growth path [15]. The interaction between plants, roots, and their environment in search of nutrients [16]

has been labeled “plant intelligence” [17]. Zhou et al. expanded on the application of plant intelligence to integrate 3D printed structures with plant roots via inosculation (the combination of multiple roots or branches into one “glued” structure) to create a hybrid ELM self-sustaining 3D structure [18]. The systematic exploration performed in developing these 3D structures expanded the capabilities of the EPRMs. Nevertheless, little is known about the mechanical properties of these materials.

The lack of information available on the mechanical properties of EPRMs delimits their application potentials in design. When it comes to living materials, this understanding can be achieved through a combination of mechanical tests (see, for example [10,19]). Interwoven is a novel EPRM, so there is no precedent to dictate how it should be characterized. However, the random distribution of roots throughout the EPRM is analogous to the structure of fibers in non-woven textiles [20]. More specifically, the structures formed by the random orientation of roots resemble electro-spun fibers [21–23], so the test methods used for non-woven textiles were taken as the basis for characterizing these EPRMs. The dependence of the microstructure and performance on the processing parameters is unclear, and understanding this relationship is essential to finding a suitable application. This knowledge gap is addressed by designing samples with different grid patterns of which the size of the grid cell (Fig. 1) is varied as described in the specimen preparation section.

Engineered living materials aim to tailor the material properties of a living (micro)organism through physical or genetic manipulation. This work characterizes the properties of a physical ELM grown from plant roots. Through mechanical testing and digital microscopy, new light is shed on the interactions that occur between roots when forming EPRMs. The effects of different root configurations and structures on stiffness and tensile strength are analyzed in a comparative study. The introduction of agar-agar improves the mechanical properties by acting as a biopolymer matrix. The resulting “green composite” uses the root structure as a natural fiber reinforcement [24].

Table 1
Examples of plants used in biodesign.

	Rootbound by Diana Scherer is a dress made from Interwoven plant root material. The piece was displayed in the Fashioned from Nature exhibition at the Victoria & Albert Museum.	https://carolineobreen.com/diana-scherers-in-victoria-albert-museum-london/
	Baubotanik by Dr. Ferdinand Ludwig are living buildings that fuse man-made scaffolds with trees, creating a hybrid ELM structure.	https://www.archdaily.com/775884/baubotanik-the-botanically-inspired-design-system-that-creates-living-buildings
	Living Root Bridges by the Khasi and Jaintia tribes of Meghalaya are bridges whose structure and strength grows with the roots over time.	https://www.brokennature.org/living-root-bridge-ecosystems-india
	Fullgrown by Alice and Gavin Munro is a company that grows furniture from trees that are pruned and “trained” to fit the shape of the desired product.	https://fullgrown.co.uk

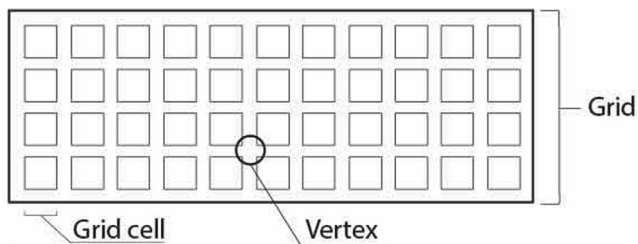


Fig. 1. Nomenclature for the different parts of the root structure.

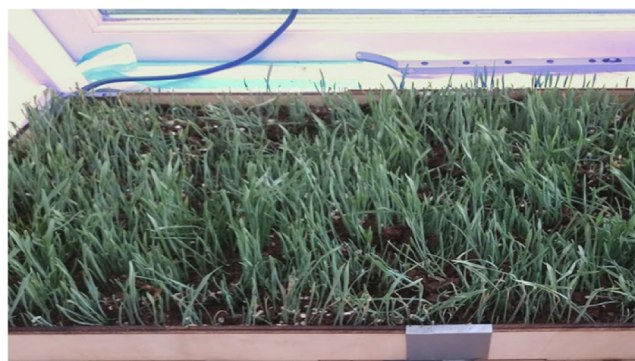


Fig. 2. Setup for growing EPRMs under a growing light.

2. Materials and methods

2.1. Plant growth Setup

Plant root materials were grown according to Diana Scherer's proprietary methods. Oat seeds (*Avena Sativa*) (van der Wal Beheer

B.V., NL) were cultivated on a window sill (Fig. 2) for 14 days under a combination of natural light and a growing light (Mars Hydro Pro II Epistar 80, 165 Watt) for 8 h per day. The plant setup had three components: (1) a digitally fabricated (i.e. 3D printed or laser cut) template to guide the root growth, (2) Forflora universal potting soil, and (3) 0.27 g/cm² of seeds. Three different templates with predefined square grids were used. For each template, the cell size was different: 0.5 cm, 1 cm, and 2 cm (Fig. 3).

2.2. Specimen preparation

Tests were performed on five different root configurations to quantify the effects of (micro)structure on mechanical performance. The root configurations tested include three "root structures" (grids with cells either 0.5 cm, 1 cm, or 2 cm in length), individual roots, and a biopolymer-matrix composite made from agar-agar and a 1 cm root grid. After 14 days of growth, three tensile coupons were cut out from each planar grid grown in each template. Since, there is no standard procedure for testing the properties of these EPRMs, the coupon dimensions of 25 mm × 150 mm were taken from the American Society for Testing and Materials (ASTM) standard "Test method for breaking force and elongation of textile fabrics" (ASTM D5035) [25]. All samples were conditioned to ensure equivalent levels of moisture by drying at least 24 h in the same environment they were to be tested according to the standard "Practice for conditioning and testing textiles" (ASTM D1776) [26].

The samples for testing the individual root and composite configurations required extra steps in preparation. Continuing the analogy of non-woven textiles, the properties of individual roots in the structure were tested according to ASTM D3822 - the standard "Test method for tensile properties of single textile fibers" [27]. Six individual root samples with a length of at least 20 mm were extracted from a grid structure. Six agar-agar composite sam-

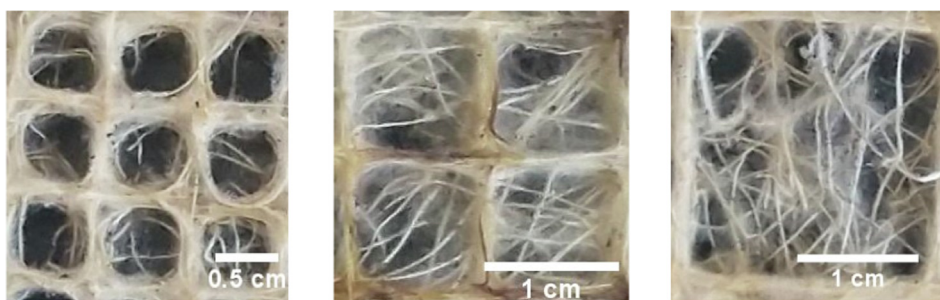


Fig. 3. EPRM grown from *Avena Sativa* into grids with three cell sizes: (a) 0.5 cm (b) 1 cm (c) 2 cm.

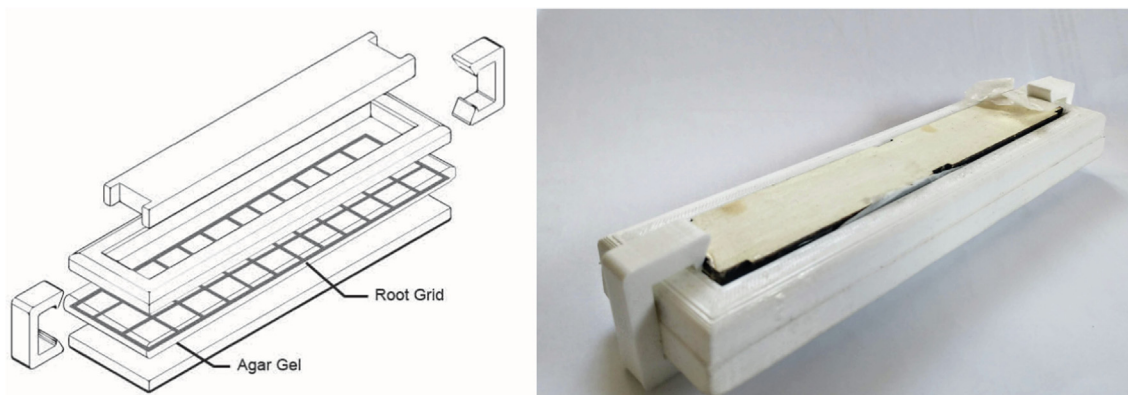


Fig. 4. Clamp used for composite tensile samples.

ples were tested according to the “Test method for tensile properties of polymer matrix composite materials” (ASTM D3039) [28].

As a proof of concept to improve tensile properties, agar-agar composites were produced with one of the templates. Agar-agar is a gelling agent whose stiffness varies with the concentration of the solution used. This study used a gel prepared with a ratio of 8 g agar-agar powder (Jacob Hooy & Co BV, Limmen, NL) to 1 L of water. To prepare the solution, the powder was dissolved in boiling water. As the solution cooled, it was poured into a mold that had an outstretched 1 cm root grid coupon with the same dimensions as above (Fig. 4). After five days of drying at room temperature, the samples were removed from the mold as a thin, uniform coupon.

3. Mechanical testing

Three specimens of each root structure (Fig. 5) were tested with a Zwick/Roell Z010 universal testing machine (Ulm, Germany) applying a cross-head velocity of 15 mm/min (10 % of the sample length) and a 1 kN load cell. After testing, a Keyence® VHX-7000 (Mechelen, Belgium) digital microscope was used on the cross section of the samples to determine fiber density and identify microstructural properties. This allows for a more accurate representation of the effective cross sectional area while taking the porosity of the samples into consideration.

The individual roots were tested using a dynamic mechanical analyser DMA Q800 (TA Instruments, Newcastle, DE, United States) in tensile mode (Fig. 6). This test mode was configured with a displacement equal to 10 % of the gauge length of each sample in accordance with the standard [27].

3.1. Root tip density

The differences in mechanical responses were corroborated with a microscopic analysis of the samples. The aforementioned Keyence® digital microscope was used to view the points of intersection between cells (henceforth referred to as vertices as defined in Fig. 2). The yellow tips of individual roots were seen accumulating at the vertices of all root structures, so they were identified as a microstructural phase of interest. In order to identify any possible

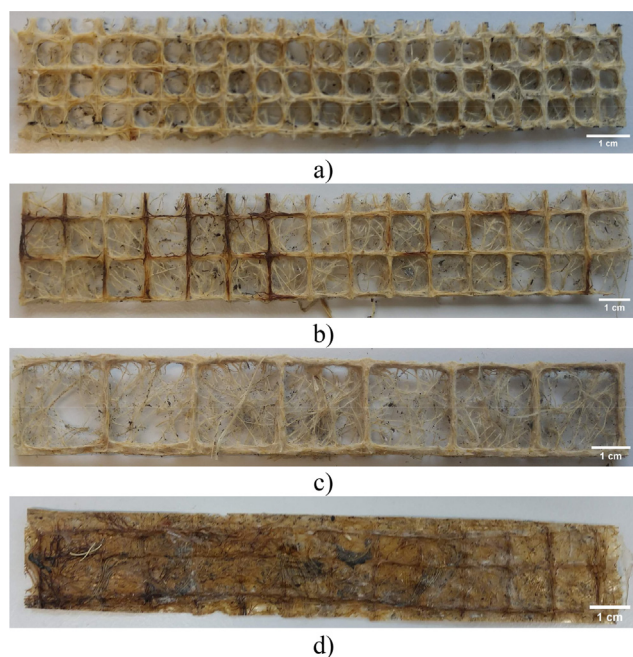


Fig. 5. Tensile test specimens for a) 0.5 cm b) 1 cm c) 2 cm and d) agar.

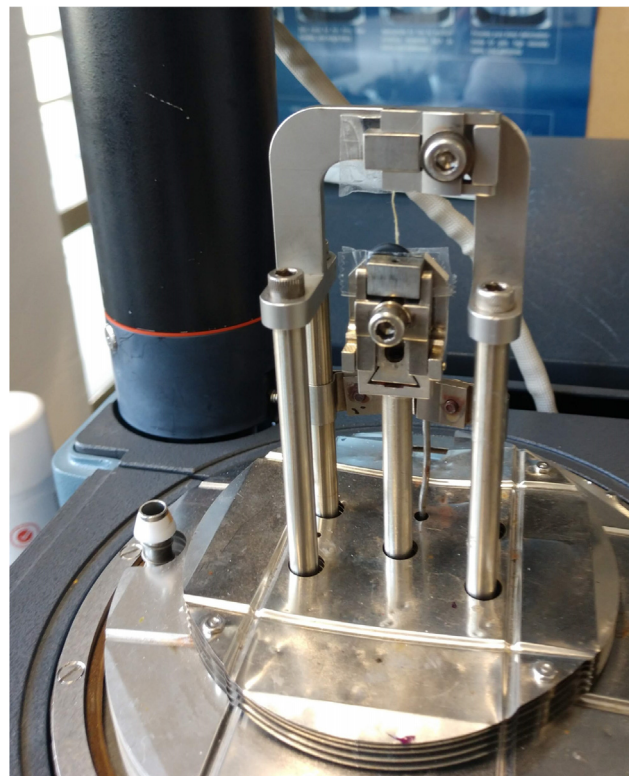


Fig. 6. Setup for testing the tensile strength of a single root.



Fig. 7. Microstructural root tips identified in the vertex of a 2 cm grid. The arrows point to the yellow root tips. (For interpretation of the references to colour in this figure legend, the reader is referred to the web version of this article.)

correlation between the characteristics of the microstructure and mechanical properties, all vertices in each root structure's tensile coupon were studied under the microscope. A constant magnification of 50x was used to count the number root tips present (Fig. 7). The average number of root tips per vertex (i.e. root tip density) was then calculated for each sample and represented by the value ρ_{tip} .

3.2. Density measurements

3.2.1. Material density

The density of each sample was derived from its mass and effective volume. Assuming that the individual roots approximate a cylinder, the volume was calculated from the diameter and length of the specimens. Unlike the roots, however, the root structures had varying degrees of porosity. The degree of porosity was calculated by looking at individual cells under the Keyence® microscope. The microscope’s postprocessing software can differentiate between “phases” in an image (i.e. pores and roots) according to brightness levels and calculate the area fraction taken up by each. Using this software, the area fraction taken up by roots (v_f) in the grid cell was calculated.

Fig. 8 illustrates this calculation. The red square in the image delineates the total area measured, whereas the dark spots (porosity) are excluded from the calculation. The resulting fraction, v_f is used to calculate material density as follows:



Fig. 8. Example of a 1 cm cell used to calculate volume factor.

$$\rho = \frac{m}{L \cdot w \cdot t \cdot v_f}$$

where:

ρ - density [kg/m ³]	L - gauge length [m]
w - width [m]	v_f - volume factor [%]
m - mass [kg]	t - thickness [m]

3.2.2. Cross-sectional fiber density

The volume factor that was calculated for each specimen, v_f , is a bulk property that is evaluated at the surface of the sample. To better represent the load-bearing capacity of the tensile coupons that were tested, a similar measurement was performed on their cross sections. After testing, the samples were cut into thirds and the four cross-sections produced by the cuts were analysed under the microscope. Each cut produced two types of cross sections whereby the roots were either horizontally or vertically oriented (with respect to the loading direction) as seen in Fig. 9.

The porosity in the cross-sections was accounted for with a correction factor a_f (similar to v_f). This correction factor is an average of the fractional area covered by each of the four cross-sections per sample. Though the vertically oriented root bundles are aligned with the loading direction, it is unclear how the load is distributed throughout the cross-section, so the average accounts for both orientations. The procedure to calculate a_f is illustrated in Fig. 10 with a horizontal root cross section as an example. An estimation of the load-bearing cross-sectional area of each sample was then calculated with the equation below - where w and t are the average of three measurements of width and thickness, respectively.

$$A_{eff} = w \cdot t \cdot a_f$$

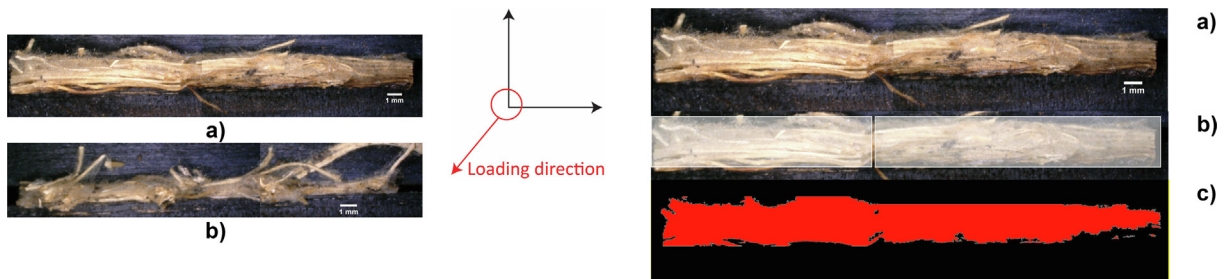


Fig. 9. Cross sectional micrograph with a) horizontally and b) vertically oriented roots with respect to the loading direction.

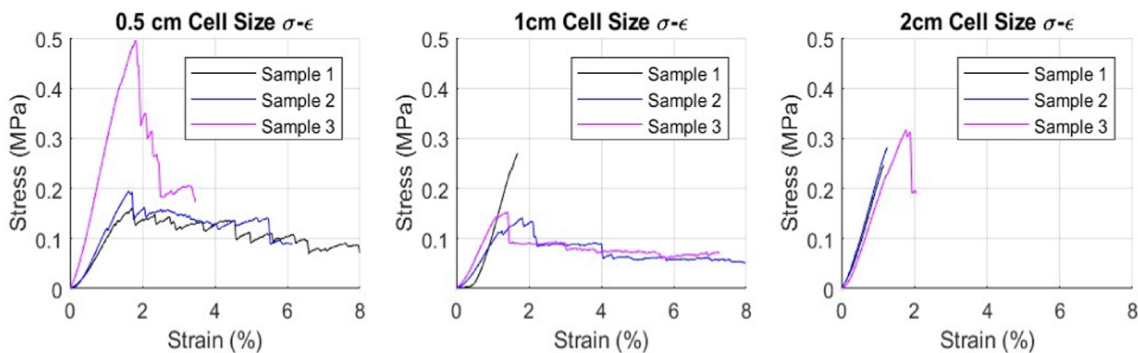


Fig. 10. Measuring the area factor - a) Horizontal root cross section b) selected area of interest c) effective cross sectional area.

4. Mechanical property calculations

Stress–strain plots were derived from the force–displacement data recorded during the tensile tests. These plots were then used to calculate tensile properties such as yield strength, tensile strength, elongation at break, and axial stiffness. The former three properties are all derived from stress–strain curves. Axial stiffness is dependent on the material's structure and is not an intrinsic material property. The stiffness is an indication of how much a sample resists deformation under a load and is derived from the force–displacement curve. Young's Modulus was also calculated, but only for individual roots and composite samples. This value is similar to stiffness, but it is an intrinsic material property derived from the stress–strain curves.

4.1. Stress

Tensile tests measure how much a sample elongates under a force, but the intention is to monitor the strain as a response to the applied stress. Converting the force–displacement data to stress–strain normalizes the data so as to allow to compare material properties regardless of the sample dimensions. Uniaxial engineering stress is defined as $\sigma_{\text{eng}} = F/A$, where the force response is divided by the cross sectional area of the sample (usually calculated by the width*thickness). In this study, A is overestimated with this calculation, which is why the a_f was used as a correction factor. The effective cross sectional area $A_{\text{eff}} = A * a_f$ is used to calculate the σ_{eng} values as well as the axial stiffness of each sample.

4.2. Axial stiffness

Axial stiffness is an extrinsic (dimension-dependent) property that describes a material's response to uniaxial loading. All root structures are made from the same material (roots) that is arranged according to the template they were grown on, so any differences in mechanical properties will not be intrinsic to the material. The axial stiffness k can be used to describe any perceived differences and is calculated according to Hooke's Law, seen below:

$$k = \frac{A_{\text{eff}} E_{\text{root}}}{l_0}$$

The axial stiffness (N/mm) of each root configuration was calculated with the effective cross-sectional area A_{eff} , the elastic modulus for roots, E_{root} , and the gauge length l_0 .

4.3. Young's modulus

Young's modulus (E) is an intrinsic (dimension-independent) property that should be the same regardless of the root configuration in the samples. It is calculated from the slope of the linear-elastic region of a stress–strain curve. In this case, E_{root} is calculated from the DMA curves. However, since E is a material property, the introduction of an agar-agar matrix to form composite coupons invalidates the use of E_{root} . Instead, the Young's modulus for these composites E_{agar} is calculated from the stress–strain curves obtained. This value was then used in the axial stiffness calculations of the composites.

4.4. Yield and tensile strength

Conventionally, the Yield Strength is the stress at which permanent deformation of a sample begins and is delineated by the end of the linear-elastic region. When used in design, this point is typically avoided to ensure that the design is not permanently deformed to unintended dimensions. Since the exact point at

which the linear-elastic region is not easy to quantify, it is calculated by drawing a curve with the same slope as the modulus slightly to the right of the sample's curve. A 0.2 % strain offset was used here, and the intersection between the two curves was taken as the yield strength.

The tensile strength of a sample is easily read off of the stress–strain curve as the highest point in the curve (i.e. its maximum). In engineering materials, this is the point at which necking occurs and a sample begins to fail/rupture.

4.5. Elongation

The horizontal axis of a stress–strain curve refers to strain, defined as a ratio of displacement-to-gauge length. Gauge length, l_0 is the original length between the clamps in a tensile machine. This value was 75 mm for all tensile coupons, but l_0 for individual roots varied with the length of the root. The amount of elongation at failure is usually taken as an indication of how malleable or flexible a material is. This point of final elongation is taken as the final point on the horizontal axis.

5. Statistical analysis

Statistical analyses were performed on the retrieved data to evaluate the significance of the results. An analysis of variance (ANOVA) was performed on the axial stiffness, yield strength, and elongation at break of all root configurations, as well as the root tip density of each structure. The ANOVA values were then used for a post-hoc Tukey's range test ($p \leq 0.05$, $n \geq 3$), where p is probability number and n is the number of samples.

6. Results

6.1. Root configurations

Of the five root configurations tested, the single root configuration was strongest. It was three orders of magnitude stronger than the 2 cm cell structure, which was the strongest of the root structures. The average yield and tensile strength of single roots were 99.67 ± 52.129 MPa and 124.750 ± 53.238 MPa, respectively. The same values for the 2 cm cell grids were 0.234 ± 0.018 MPa and 0.281 ± 0.036 MPa (Fig. 11 and Table 2).

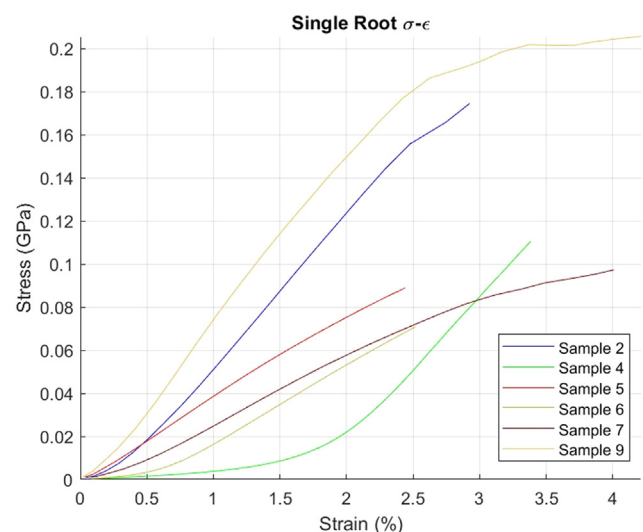


Fig. 11. Stress–strain curves for each cell size.

Table 2

Overview of root configuration properties (\pm standard deviation). Letters indicate statistically significant differences with corresponding configurations at $p \leq 0.05$.

Configuration	Fiber volume (%)	Density (g/cm ³)	Axial stiffness (N/mm)	Yield strength (MPa)	Tensile strength (MPa)	Elongation at break (%)	Root tips per mm ²
0.5 cm cell ^a	74.04 \pm 13.26	0.176 \pm 0.025	17.45 \pm 5.83 ^{d,e}	0.171 \pm 0.064 ^{d,e}	0.283 \pm 0.184 ^{d,e}	7.356 \pm 4.632 ^{d,e}	0.1365 \pm 0.070 ^{b-c}
1 cm cell ^b	76.42 \pm 8.89	0.125 \pm 0.011	19.95 \pm 2.84 ^{d,e}	0.163 \pm 0.063 ^{d,e}	0.189 \pm 0.072 ^{d,e}	5.752 \pm 3.554 ^{d,e}	0.1354 \pm 0.068 ^a
2 cm cell ^c	75.13 \pm 11.15	0.116 \pm 0.006	23.75 \pm 4.46 ^{d,e}	0.234 \pm 0.018 ^{d,e}	0.281 \pm 0.036 ^{d,e}	1.486 \pm 0.485 ^{d,e}	0.5677 \pm 0.181 ^a
Agar ^d	1.00	0.259 \pm 0.045	0.784 \pm 0.191 ^{a-c,e}	2.236 \pm 1.151 ^{a-c,e}	3.308 \pm 1.191 ^{a-c,e}	8.409 \pm 10.272 ^{a-c,e}	
Single root ^e	1.00	2.342 \pm 0.841	0.027 \pm 0.012 ^{a-e}	99.667 \pm 52.131 ^{a-e}	124.75 \pm 53.238 ^{a-e}	3.249 \pm 0.750 ^{a-e}	

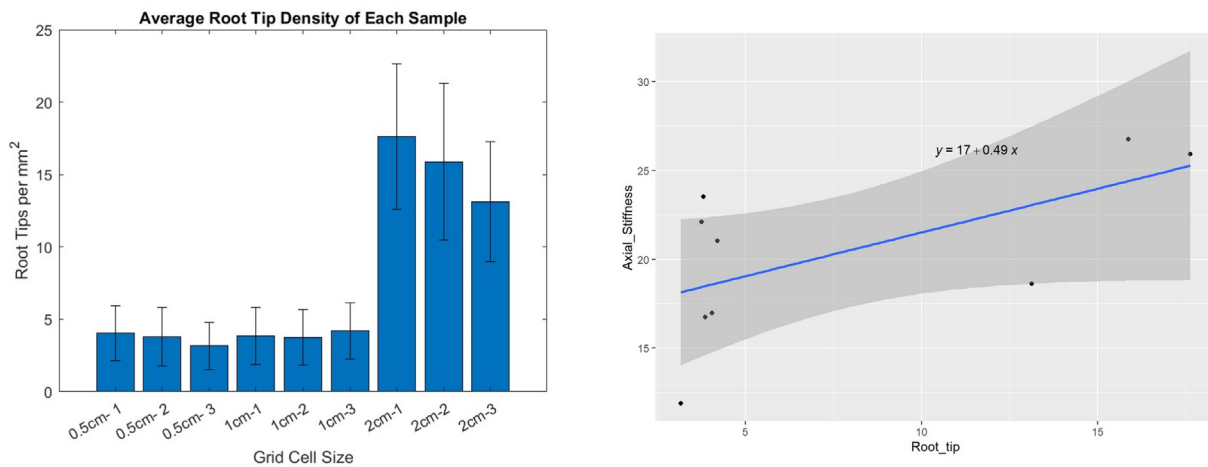


Fig. 12. Single root stress-strain curves (from DMA).

6.2. Single roots

The elastic modulus of individual roots, E_{roots} , was calculated from the slope of the curves seen in Fig. 12. The average value for E_{root} , was 54.10 ± 19.88 MPa. This average is the value used in the calculation of axial stiffness.

6.3. Axial stiffness

A glance at Table 2 suggests the 2 cm coupons were the stiffest, while the 5 mm coupons were the least stiff root structures (23.7

5 ± 4.46 N/mm and 17.45 ± 5.83 N/mm, respectively). However, Fig. 11 shows how Sample 1 of the 5 mm coupons had a comparable tensile response to the strongest 2 cm coupons. Given this large spread of the data and limited sample size, statistical analysis revealed that these averages cannot be considered different with a statistical reliability of 95 %. On the other hand, the stiffness of the agar-agar coupons and the single roots were much smaller because of dimensional differences (recall that stiffness is an extrinsic property).

6.4. Root tip density

The average root tip density of each sample, ρ_{tip} , varied within each root structure and could be correlated to the axial stiffness (Fig. 13). The root tip density of the 2 cm cell grid was 4 times that of the other structures with an average of 0.568 ± 0.181 root tips / mm², while that of the 0.5 cm and 1 cm grid cells was 0.137 ± 0.070 (24.12 %) and 0.135 ± 0.068 (23.76 %) root tips/mm², respectively. The latter two densities were not statistically different from each other, as can be corroborated from Fig. 13a. The linear regression in Fig. 13b suggests a possible correlation between root tip density and axial stiffness, but the correlation between ρ_{tip} and structure is less evident.

6.5. Agar-Agar matrix composites

Agar-agar was introduced to a 1 cm cell grid as a biopolymer matrix with the intention of improving the performance of the root structure. When compared to the 1 cm root structure, the agar-agar matrix increased the average yield and tensile strengths by an order of magnitude to 2.23 ± 1.151 MPa and 3.308 ± 1.191 Mpa, respectively (Fig. 14). The slope of the linear elastic area of the curves in Fig. 14 was used to calculate E_{agar} , and thus, axial stiffness. Note that, while there are two samples that overlap

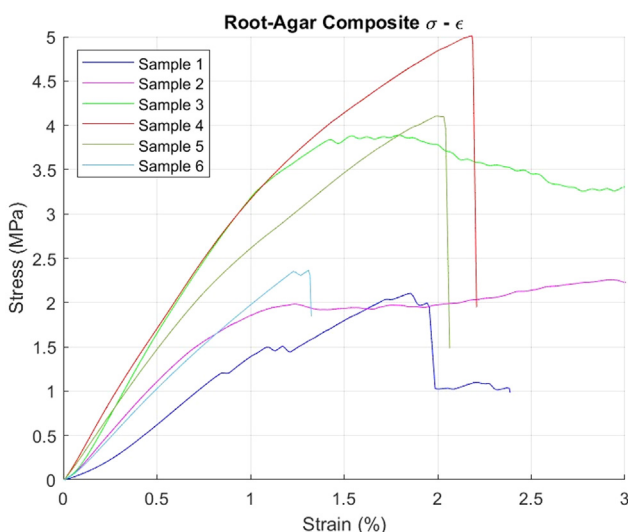


Fig. 13. Average root tip density a) per sample and b) correlated with axial stiffness (linear regression).

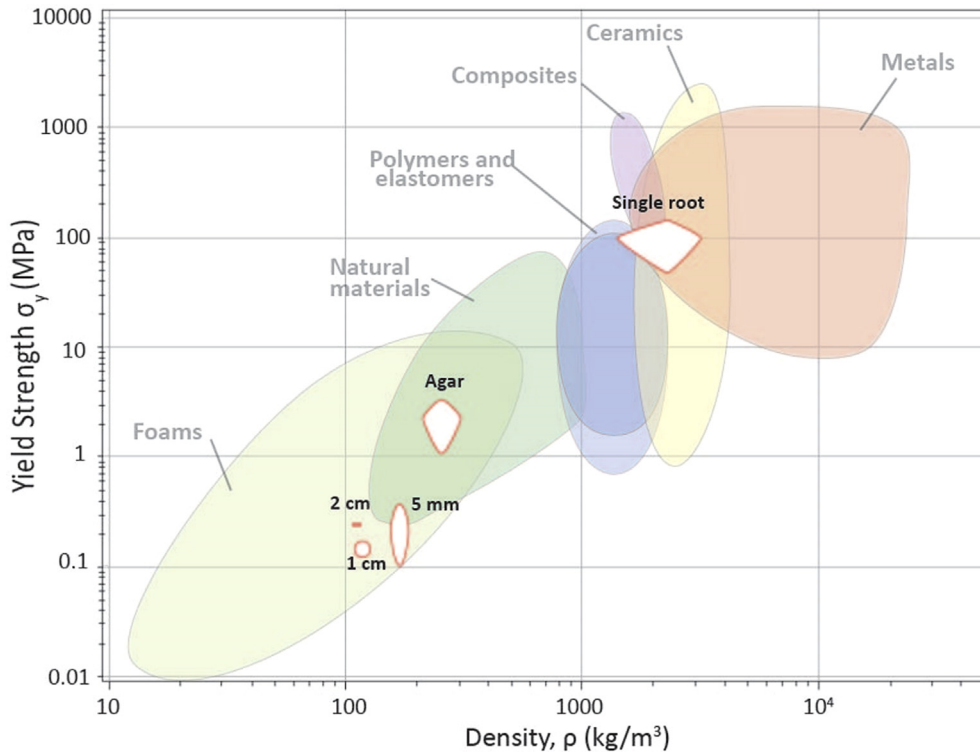


Fig. 14. Stress–strain curves for the composite samples.

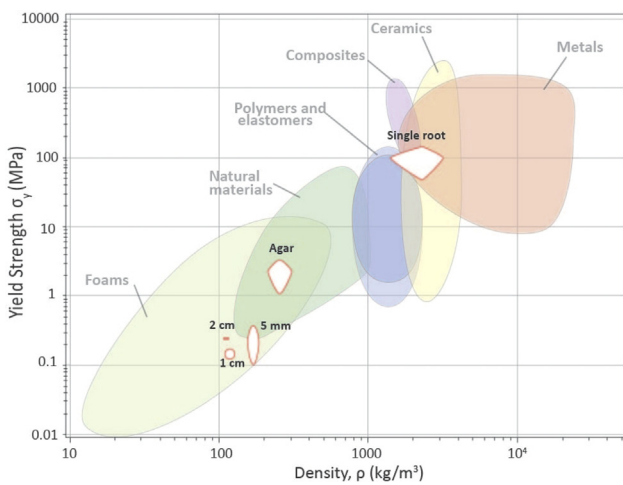


Fig. 15. Yield-density curve adapted from [30] with the current work’s data superimposed to compare EPRMs to other materials.

almost exactly, and there is still plenty of differences in performance, the slope of $E_{\text{agar}} = 2.705 \pm 0.571$ MPa exhibits less scatter for the Agar-Agar Matrix composites than the pure roots structures.

6.6. Density

The density values had an inverse relationship with the size of the grid’s cells (i.e. the largest cell size was the least dense). The addition of agar-agar not only improved load distribution, but it also effectively doubled the density of the composite to 0.259 ± 0.045 g/cm³. Finally, the single root was the densest configuration with a density of 2.342 ± 0.841 g/cm³. This range in densities were all plotted in the yield strength-density curve seen in Fig. 15 to

show how the plant root materials compare to more common engineering materials. With minimal differences in density, the three root structures behave mainly like foams do, likely because of their high porosity.

The increased performance in agar composites best compares to other natural materials and some foams, but the individual roots are the ones that best hold up with other engineering materials. The large spread in data places its properties anywhere between polymers and elastomers to ceramics and composites. This is consistent with other plant fiber reinforced composites, which are becoming increasingly attractive because of their high specific strength (strength/density) [29].

7. Discussion

The characterization of the ERPMS suggests a connection between microstructure, root configuration and mechanical performance. From the microscopic analysis, it is clear that changes in the root configuration affect the root tip density at grid vertices. Root tips are a microstructural feature whose presence was largest in the most stiff root structures, which could be used as an indication of mechanical strength in an EPRM. The mechanical strength of the material is strongly dependent on load distribution within the root structure, of which the root tip density at vertices represents a crucial structural parameter. However, the relationship between the root configuration and the root tip density remains unclear due to the stochastic nature of the material. Though the 2 cm cells produced the stiffest structures and the highest root tip density, the correlation between ρ_{tip} and axial stiffness shown in Fig. 13b is not statistically significant with a statistical reliability of 95 %. Because of the small sample size of each root structure, it is difficult to identify outliers as such within the given data set. Assuming the perceived positive correlation is true, the precise functional relation between ρ_{tip} (as an aggregate structural parameter) and the mechanical strength remains unknown. Deciphering

the relationship between root configuration and root tip density is key for designing the properties of plant root materials. Further investigation is necessary to clarify the role of a vertex with more root tips in defining mechanical strength. A vertex with more root tips could be an indication of complex root entanglement, or it could hint towards more roots being present in the root structure. Though its detailed exploration exceeds the scope of this investigation, it should be noted that there might be a biological explanation behind the observed phenomena.

More roots in the structure do not necessarily translate to a stronger material. In fact, a higher density was associated with smaller cell size and it led to a lower axial stiffness. Root structures are composed of an entanglement of root networks that transfer a load between them when pulled. The entanglement of roots at a vertex plays an important role in performance, but it has not been thoroughly studied yet. When performing tensile tests, the clamps pull on (at least) two separate root networks that are loosely linked by other intermediate networks. The load transfer between these networks is less efficient than pulling on one individual root. Individual roots were much stronger than any of the root configurations tested because the test was performed on a structure that was unified at both ends. By pulling on one single root (rather than a network), the load distribution remains uniform. The loss of efficiency observed when dealing with a root network hints at the complexity of root-to-root interactions, especially at the vertices. Each observed root tip is a part of its own entangled network, yet it is still unclear how a uniaxial load is transferred from one end to the other, given the complex nature of the network. A precise quantitative understanding on how the root structure responds to an external load will require (i) a precise knowledge on the organic interconnectivity of the root structure and (ii) an accurate numerical model (such as e.g. a Finite Element model) to calculate how loads are distributed over the structure.

The agar-agar matrix also affects mechanical behavior. Agar-agar proved to be a suitable strengthening mechanism because it increases density and eliminates the high porosity of the root structures. The matrix distributes the tensile load more uniformly throughout the test coupon, which further implies that the low performance seen in the root structures are a consequence of poor load distribution. Despite the increase in strength, it is unclear how the presence of agar-agar impacts the microstructure. Once poured over the root structure, the agar-agar gel inevitably alters root tip interactions. Further research on the microstructure of these composites is necessary to verify the effect of root tip density ρ_{tip} on mechanical properties since they are one of the parameters in EPRM processing that can be tuned through design.

8. Future work

The exploratory investigation presented here was focused on only changing two design variables in the production of EPRMs - root structure design (cell size) and composite design. There are many more parameters to be studied. Scaling up the size of the grid is likely to yield different results, while increasing the number of samples tested will increase the statistical reliability of the data. Since the templates for the root structure design are digitally fabricated, the form freedom available when designing plant root materials is vast. Changes in the template pattern (whether it be non-uniform cell sizes or a more organic pattern) must also be studied to fully understand the potential for these materials. Composite design was only introduced to test the improvements that a solid matrix would provide to the root structure's properties (this is why only one root structure was tested). There is much more to be explored in the composite design, such as the type of matrix used, matrix concentration (of agar, for example), and the impact

of different cell sizes on the composite's properties. Finally, there are likely other parameters that were outside of the scope of this exploration, namely those leading towards a better understanding of the biological factors that determine the EPRMs properties, that will inevitably impact the relevant design parameters in future studies.

Both root structure design and composite design can be altered to tune the mechanical properties of EPRMs, to a degree. There is not enough information on why or how root tip density improves the mechanical properties. Understanding this relationship is key to designing the properties of the material. Once it is possible to control root tip density across the root structure, advanced modeling techniques (such as finite element methods) can be paired with digital fabrication to fully customize the properties of these plant root materials.

9. Conclusions

This study characterizes the properties of plant root materials through a series of tensile tests and digital microscopy. The characterization systematically follows the standard testing methods for non-woven textiles, whose structure is analogous to that of the EPRMs. The load distribution of the root structures is much poorer than that of single roots because of the interactions between roots. The introduction of a biopolymer matrix vastly improves the mechanical properties because of better load distribution. Root tips were identified as a microstructural phase whose presence is an indicator of relative strength between samples. The 2 cm root structures that had the highest root tip density (0.568 ± 0.181 roots/mm²) also had the highest yield strength of 0.234 ± 0.018 M Pa. While the role of root tips in forming the strength of the EPRMs is not yet fully defined, they are paramount for designing their material properties. Since root structure design impacts root tip density ρ_{tip} and composite design improves load distribution, both parameters can be used to tune the properties of the EPRMs and improve their feasibility as alternatives to conventional foams and/or other natural materials with similar properties.

Glossary.

- **Engineered Plant Root Material (EPRM)** - planar plant root grids developed with the Interwoven method developed by Diana Scherer.
- **Root configuration** - design parameter that controls root entanglement in EPRMs, ranging from an individual root to the various networked root structures.
- **Root structure** - planar network of roots grown into a predefined pattern using the Interwoven method (in this work: 0.5 cm, 1 cm, and 2 cm cell grids).
- **Grid structure** - root structure patterned with a grid of squares grown in one of three templates.
- **Cell** - a single square unit from the grid structure.
- **Vertex** - point of intersection between multiple cells.

Funding

This research did not receive any specific grant from funding agencies in the public, commercial, or not-for-profit sectors.

Data Availability

The raw/processed data required to reproduce these findings cannot be shared at this time due to technical or time limitations, but it will be made available by the corresponding author upon request.

CRediT authorship contribution statement

Israel A. Carrete: Conceptualization, Methodology, Validation, Formal analysis, Investigation, Data curation, Writing – original draft, Writing – review & editing, Visualization, Project administration. **Sepideh Ghodrati:** Conceptualization, Methodology, Writing – review & editing, Supervision, Project administration. **Diana Scherer:** Conceptualization, Methodology, Writing – review & editing, Supervision, Project administration. **Elvin Karana:** Conceptualization, Resources, Writing – review & editing.

Data availability

Data will be made available on request.

Declaration of Competing Interest

The authors declare that they have no known competing financial interests or personal relationships that could have appeared to influence the work reported in this paper.

Acknowledgements

The authors would like to thank Professor Leo Kestens (Ghent University) for his advice about interpreting the microscopic phases of the roots alongside their tensile test results, the 3 mE department at TU Delft for granting access to their digital microscopes, and the members of Applied Labs (TU Delft, IDE faculty) for granting access to their facilities and support in using the tensile tester.

Appendix A. Supplementary material

Supplementary data to this article can be found online at <https://doi.org/10.1016/j.matdes.2022.111521>.

References

- [1] A.Y. Chen, C. Zhong, T.K. Lu, Engineering living functional materials, *ACS Synth. Biol.* 4 (1) (Jan. 2015) 8–11, <https://doi.org/10.1021/sb500113b>.
- [2] P.Q. Nguyen, N.-M.-D. Courchesne, A. Duraj-Thatte, P. Praveschotinunt, N.S. Joshi, Engineered Living Materials: Prospects and Challenges for Using Biological Systems to Direct the Assembly of Smart Materials, *Adv. Mater.* 30 (19) (May 2018) e1704847.
- [3] C. Gilbert, T. Ellis, Biological Engineered Living Materials: Growing Functional Materials with Genetically Programmable Properties, *ACS Synth. Biol.* 8 (1) (Jan. 2019) 1–15, <https://doi.org/10.1021/acssynbio.8b00423>.
- [4] M. Haneef, L. Ceseracciu, C. Canale, I.S. Bayer, J.A. Heredia-Guerrero, A. Athanassiou, Advanced Materials From Fungal Mycelium: Fabrication and Tuning of Physical Properties, *Sci. Rep.* 7 (Jan. 2017) 41292, <https://doi.org/10.1038/srep41292>.
- [5] F. Ludwig, H. Schwertfeger, O. Storz, Living systems: Designing growth in baubotanik, *Archit. des.* 82 (2) (Mar. 2012) 82–87, <https://doi.org/10.1002/ad.1383>.
- [6] W. Myers, *Bio Design: Nature, Science, Creativity*, Thames & Hudson, 2018 [Online]. Available:.
- [7] S. Camere, E. Karana, Fabricating materials from living organisms: An emerging design practice, *J. Clean. Prod.* 186 (Jun. 2018) 570–584, <https://doi.org/10.1016/j.jclepro.2018.03.081>.
- [8] Silvia-DforDesign, “Sustainable design: biofabrication is the answer,” DforDesign, Jun. 14, 2019. <https://dfordesign.style/blog/sustainable-design-biofabrication-is-the-answer> (accessed May 31, 2022).
- [9] W.D. Jang, J.H. Hwang, H.U. Kim, J.Y. Ryu, S.Y. Lee, Bacterial cellulose as an example product for sustainable production and consumption, *Microb. Biotechnol.* 10 (5) (Sep. 2017) 1181–1185, <https://doi.org/10.1111/1751-7915.12744>.
- [10] F.V.W. Appels, S. Camere, M. Montalti, E. Karana, K.M.B. Jansen, J. Dijksterhuis, P. Krijgsheld, H.A.B. Wösten, Fabrication factors influencing mechanical, moisture- and water-related properties of mycelium-based composites, *Mater. Des.* 161 (2019) 64–71.
- [11] M. Sawa, “The laboratory life of a designer at the intersection with algal biotechnology”, *arq, Archit. Res. Quart.* 20 (1) (Mar. 2016) 65–72, <https://doi.org/10.1017/S1359135516000191>.
- [12] F. Ludwig, W. Middleton, F. Gallenmüller, P. Rogers, T. Speck, Living bridges using aerial roots of ficus elastica - an interdisciplinary perspective, *Sci. Rep.* 9 (1) (Aug. 2019) 12226, <https://doi.org/10.1038/s41598-019-48652-w>.
- [13] S. Shankar, “Living Root Bridges: State of knowledge, fundamental research and future application,” presented at the IABSE Conference, Geneva 2015: Structural Engineering: Providing Solutions to Global Challenges, Geneva, Switzerland, 2015. doi: 10.2749/222137815818359474.
- [14] D. Scherer, Interview with Diana Scherer: Weaving roots at the interface between art, fashion and science, *Plants People Planet* 1 (3) (Jul. 2019) 142–145, <https://doi.org/10.1002/ppp3.48>.
- [15] D. Scherer, “Diana Scherer,” Diana Scherer. <http://dianascherer.nl/> (accessed May 31, 2022).
- [16] T.H. Tan, J.L. Silverberg, D.S. Floss, M.J. Harrison, C.L. Henley, I. Cohen, How grow-and-switch gravitropism generates root coiling and root waving growth responses in *Medicago truncatula*, *Proc. Natl. Acad. Sci. U. S. A.* 112 (42) (Oct. 2015) 12938–12943, <https://doi.org/10.1073/pnas.1509942112>.
- [17] S. Mancuso, A. Viola, *Brilliant Green: The Surprising History and Science of Plant Intelligence*, Island Press, 2015 [Online]. Available:.
- [18] J. Zhou, B. Barati, J. Wu, D. Scherer, E. Karana, Digital biofabrication to realize the potentials of plant roots for product design, *Bio-Design and Manufacturing* 4 (1) (Mar. 2021) 111–122, <https://doi.org/10.1007/s42242-020-00088-2>.
- [19] Brandon, “What is the Materials Science Tetrahedron (Paradigm)?,” *Materials Science & Engineering Student*, Jul. 05, 2020. <https://msestudent.com/what-is-materials-science-tetrahedron-paradigm/> (accessed May 31, 2022).
- [20] S.J.K. Adolph, in: 3 - The use of knitted, woven and nonwoven fabrics in interior textiles, Woodhead Publishing, 2009, pp. 47–90, <https://doi.org/10.1533/9781845696870.1.47>.
- [21] H. Li, W. Yang, “Electrospinning technology in non-woven fabric manufacturing”, in *Non-woven Fabrics*, in: H.-Y. Jeon (Ed.), *Non-woven Fabrics*, InTech, 2016.
- [22] A.K. Haghi, M. Akbari, Trends in electrospinning of natural nanofibers, *Phys. Status Solidi* 204 (6) (Jun. 2007) 1830–1834, <https://doi.org/10.1002/pssa.200675301>.
- [23] C. Vineis, A. Varesano, in: “14 - Natural polymer-based electrospun fibers for antibacterial uses”, in *Electrofluidodynamic Technologies (EFDTs) for Biomaterials and Medical Devices*, Woodhead Publishing, 2018, pp. 275–294, <https://doi.org/10.1016/B978-0-08-101745-6.00014-1>.
- [24] M.J. John, S. Thomas, Biofibres and biocomposites, *Carbohydr. Polym.* 71 (3) (Feb. 2008) 343–364, <https://doi.org/10.1016/j.carbpol.2007.05.040>.
- [25] D13 Committee, “Test method for breaking force and elongation of textile fabrics (strip method)”, ASTM International, West Conshohocken, PA (2019), <https://doi.org/10.1520/d5035-11r19>.
- [26] D13 Committee, “Practice for conditioning and testing textiles,” ASTM International, West Conshohocken, PA, 2020. doi: 10.1520/d1776_d1776m-20.
- [27] D13 Committee, “Test method for tensile properties of single textile fibers,” ASTM International, West Conshohocken, PA, 2020. doi: 10.1520/d3822_d3822m-14r20.
- [28] D30 Committee, “Test method for tensile properties of polymer matrix composite materials,” ASTM International, West Conshohocken, PA, 2017. doi: 10.1520/d3039_d3039m-17.
- [29] Y. Li, L. Xie, H. Ma, Permeability and mechanical properties of plant fiber reinforced hybrid composites, *Mater. Des.* 86 (Dec. 2015) 313–320, <https://doi.org/10.1016/j.matdes.2015.06.164>.
- [30] M.F. Ashby, H. Shercliff, D. Cebon, *Materials: Engineering, Science, Processing and Design*, Fourth, Butterworth-Heinemann, 2018, p. 167 [Online]. Available:.